Please cite the Published Version

Additional Information: This is an Open Access article published in Science Advances, by the American Association for the Advancement of Science.

Enquiries:

If you have questions about this document, contact openresearch@mmu.ac.uk. Please include the URL of the record in e-space. If you believe that your, or a third party's rights have been compromised through this document please see our Take Down policy (available from https://www.mmu.ac.uk/library/using-the-library/policies-and-guidelines)

ENVIRONMENTAL STUDIES

Tree dynamic response and survival in a category-5 tropical cyclone: The case of super typhoon Trami

Kana Kamimura[1]*, Kazuki Nanko[2], Asako Matsumoto[3], Saneyoshi Ueno[3], James Gardiner[4], Barry Gardiner[5,6]

In the future with climate change, we expect more forest and tree damage due to the increasing strength and changing trajectories of tropical cyclones (TCs). However, to date, we have limited information to estimate likely damage levels, and nobody has ever measured exactly how forest trees behave mechanically during a TC. In 2018, a category-5 TC destroyed trees in our ongoing research plots, in which we were measuring tree movement and wind speed in two different tree spacing plots. We found damaged trees in only the wider spaced plot. Here, we present how trees dynamically respond to strong winds during a TC. Sustained strong winds obviously trigger the damage to trees and forests but inter-tree spacing is also a key factor because the level of support from neighboring trees modifies the effective "stiffness" against the wind both at the single tree and whole forest stand level.

INTRODUCTION

Trees in forests suffer damage from severe meteorological events such as tropical cyclones (TCs) and extratropical cyclones; however, some trees survive even if almost all other trees are blown down by the wind (*1*). How do these trees survive even during a category-5 TC on the Saffir-Simpson scale (*2*)? Until now, no one has measured and reported tree dynamic behavior during such intense winds and shown why trees fail or survive in TCs. Therefore, tree response has been hidden in a "black box," which has made our understanding of the tree wind damage process in severe TCs and storms purely conjectural.

Large-scale wind damage in forests brings economic, social, and environmental losses such as reducing timber production, disrupting human activities, and changing forests from carbon sinks to carbon sources (*3–7*). In the near future, we will face more tree and forest damage due to global warming. Category 4 and 5 TCs will increase in number and migrate further north in the north hemisphere (*8–11*). Hence, forest damage will be found not only in the current TC-affected regions, mainly in East Asia and the Caribbean-Central American region, but also in forests at higher latitudes that are not acclimated to TCs.

To minimize future damage in forests, we need to be able to predict where, how, and when trees will fail during strong winds. To date, researchers have assumed a three step process: First, strong winds create a large pressure difference across the tree canopy; second, this pressure difference leads to branch oscillations and these oscillations are transferred to the stem and down into the roots (*12*); and last, the accumulated strain energy from the bent stem and roots creates cracks in the stem and roots and either breaks the root-soil plate causing uprooting or leads to stem breakage (*3, 13*). Previous research has collected data to explain these steps by field

and/or laboratory experiments and post-storm measurements; the knowledge is then used to develop mechanistic (*14–16*) and tree dynamic (*17, 18*) models of tree response to strong winds. These models also provide the possibility to predict wind damage in forests under changing TC behavior.

However, the current knowledge and models still contain many assumptions and we do not know how closely their predictions relate to real damage events. For example, the field measurements to develop these models have all been conducted under normal to strong wind conditions (mean wind speed of <10 ms^{-1} at canopy top), which is much lower than the wind speed leading to tree damage (*19*). The natural frequency of the tree has in the past been regarded as the main energy transfer mode from the wind to the tree, and this leads to damage (*3, 20*). On the other hand, a number of researchers have not found any resonant response between the main energy containing eddies in the wind and tree movement (*21, 22*). To reduce the uncertainty between our assumptions on tree response and actual tree behavior, together with understanding the factors that control this behavior, we need to monitor trees during the intense meteorological conditions, such as during a TC, that lead to damage.

In 2018, we finally succeeded in monitoring the dynamic response of trees to wind during a TC that left both damaged and undamaged trees. A category-5 TC, typhoon Trami, made landfall in Japan and destroyed trees in two ongoing research plots that were being monitored for tree movement, wind loading on the trees, and wind speed in and outside the plots. The plots consisted of genetically similar *Cryptomeria japonica* trees (full siblings), planted at the same time. One of the plots had been thinned by 50% stem removal in the previous year (named as P-50), and the other had no treatment (all stems remained from the initial planting and named as P-100). We found damaged trees only in P-50 (see movie S1). Here, we address how the trees failed or survived under these different stand conditions during the TC. We also give answers to two questions: whether the observed tree failure mechanism was a unique feature of strong TCs or is common during any strong winds, even non-TC storms, and whether tree resonant response leads to wind-caused damage in forests. Our findings are a substantial step in reducing the gaps between our current understanding of tree damage and the actual damage process and will improve our ability to predict forest wind damage and to manage forests at risk under the changing climate.

[1]School of Science and Technology, Shinshu University, Minamiminowa, Nagano, Japan. [2]Department of Disaster Prevention, Meteorology and Hydrology, Forestry and Forest Products Research Institute, Tsukuba, Japan. [3]Department of Forest Molecular Genetics and Biotechnology, Forestry and Forest Products Research Institute, Tsukuba, Japan. [4]Institute of Life Course and Medical Sciences, University of Liverpool, Liverpool, UK. [5]Faculty of Environment and Natural Resources, Albert-Ludwigs University, Freiburg, Germany. [6]Institut Européen de la Forêt Cultivée, Cestas, France.
*Corresponding author. Email: kamimura@shinshu-u.ac.jp

RESULTS

In 2017, we created two plots within a research compartment (fig. S1) with strain gauges attached to 36 trees and inertial measurement unit (IMU) sensors attached to 33 trees. In 2018, typhoon Trami damaged eight trees in the thinned area of the compartment only, including six in the P-50 plot, and we were able to obtain data from three damaged and 26 undamaged trees. We focus on the period from 2000 on 30 September 2018 to 0700 on 1 October 2018, which included the peak in wind speed during the TC.

Temporal changes of wind and tree stem angles

The wind speed started to increase after 2000 (30 September 2018; Fig. 1A), and the large-scale sweep-ejection events (23), transferring momentum into the canopy, increased in intensity (fig. S2). After

0110 (1 October 2018), the momentum flux ($u'w'$) suddenly increased in magnitude (a negative $u'w'$ indicating transfer of momentum downward into the canopy from the higher momentum air above the canopy; Fig. 1A). This rapid wind speed increase caused all the tree stems to lean much more than previously (Fig. 1B). Some of the P-50 trees started oscillating from 2030 (30 September 2018), but they still returned to their vertical rest position when the wind speed dropped (2220 to 2230 and 2300 to 2310). Trees s10, s14, and s15 in P-50 were damaged between 0110 and 0120 (Fig. 1C), matching the sudden change of the wind speed. After 0430 (1 October 2018), the P-100 trees returned to their rest position as the wind speed started to decrease, whereas the P-50 trees still reacted to even small increases in wind speeds and never returned to their vertical rest positions even after the TC had passed (they remained on average at approximately a 2% lean angle).
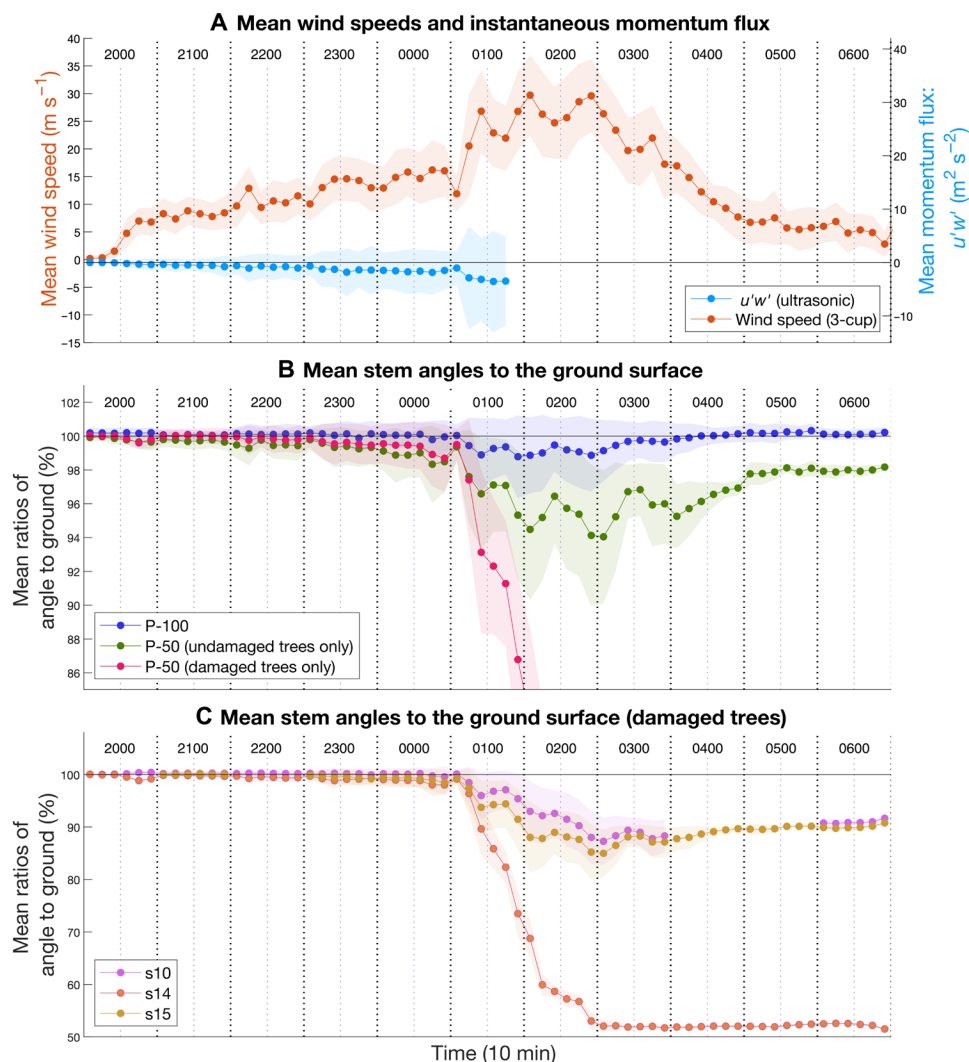

Fig. 1. Wind speeds and tree lean angles during typhoon Trami. (**A**) Ten-minute mean and SD (transparent-colored cloud behind the lines) of wind speed outside the plots (measured with a three-cup anemometer) and instantaneous momentum flux ($u'w'$) inside the plots (measured with an ultrasonic anemometer); (**B**) A 10-min averaged stem angles to the ground, which were compared to the vertical rest position (assessed between 0100 and 0200 on 28 September 2018); (**C**) A 10-min averaged stem angles of the damaged trees, which were also compared to the vertical rest positions. One-hundred percent indicates that the stem vertical position was the same as the rest position. We determined the trees as damaged if their minimum stem angles to the ground were below 83% (detailed justification is provided in Materials and Methods). The $u'w'$ line ends at 0150 because the ultrasonic anemometer was torn off the mast by the wind.

Similarity and differences in tree oscillation within and between the plots

The two-sample Kolmogorov-Smirnov tests indicated whether the trees oscillated in a similar or different manner within or between the plots by comparing all available tree-pair oscillation frequencies at the height of the crown center in two directions: north-south and east-west (Fig. 2). The height of the crown center was determined as the height from the ground surface to the initially estimated crown base at 6 m plus crown length/2. Almost all the P-100 trees oscillated similarly over the strong wind period. After 0110, 10 to 20% of the trees oscillated differently to other trees in the plot, but after 0320, when the wind speed started to decrease, they again oscillated similarly (Fig. 2B). The P-50 trees, on the other hand, started oscillating in an individual manner earlier than the P-100 trees did
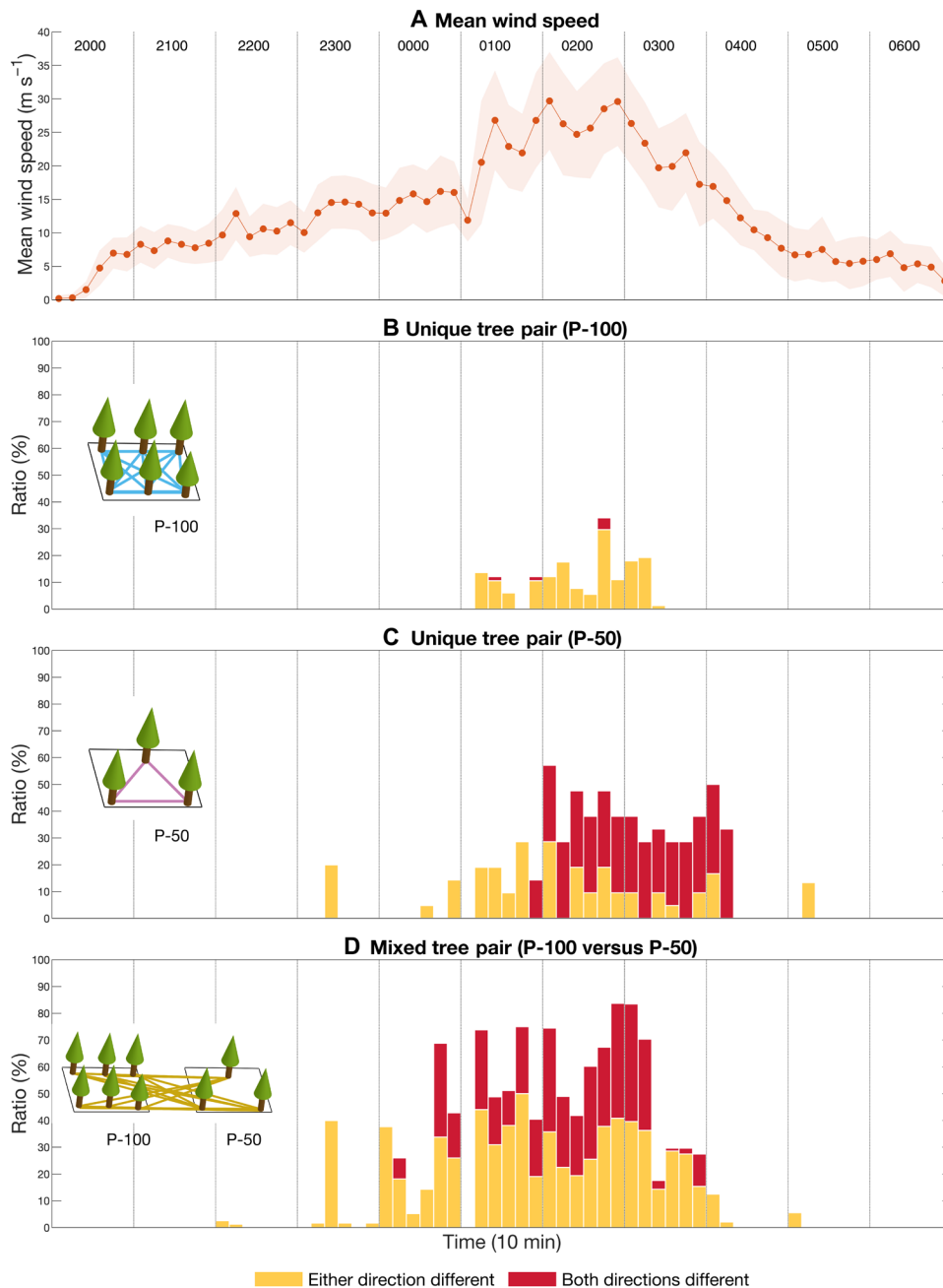

Fig. 2. Similarity or difference of tree oscillation within or between the plots. All paired trees (see the images on the left side) were tested using the two-sample Kolmogorov-Smirnov tests (at the 0.05 significance level) with the frequencies of the tree movement (at 0.1-m distance intervals during every 10 min in two directions), north-south and east-west, from 2000 (30 September 2018) to 0700 (1 October 2018): (**A**) 10-min mean wind speed outside the plots (same as in Fig. 1A); (**B**) tested P-100 tree pairs [the numbers of tree pairs every 10 min (n_{pair}) being between 55 and 91]; (**C**) tested P-50 tree pairs (n_{pair} between 6 and 21); (**D**) tested between the P-100 and P-50 trees (n_{pair} between 24 and 49). The graphs indicate if the tree pair oscillated in a different manner in one direction (orange color), if the tree pair oscillated in a different manner in both directions (red color), and if the tree pair oscillated similarly in both directions (no color).

(Fig. 2C). In particular, tree s15 (damaged tree) started oscillating differently when the mean wind speed reached approximately 10 ms^{-1} outside the plots. After 0000, most of the P-50 trees behaved differently from the P-100 trees (Fig. 2D) except trees s01 and s13 (both undamaged in P-50), which tended to oscillate in a similar manner to the P-100 trees.

Dynamics of individual tree oscillations

Focusing on the time with the rapid increase in wind speed (every 10 min from 0100 to 0130 on 1 October 2018), we observed that when wind speeds declined in the first period (0100 to 0110), the crown centers moved only within 1 m of the tree vertical rest positions (the origin in the plots in Fig. 3). The maximum turning moments (TMs) measured at the tree stem base were also lower than those in the other periods (<0.5 × 10^4 Nm). When the wind speeds increased rapidly in the second period (0110 to 0120), all the trees started to oscillate with a large magnitude. In particular, trees s14 and s15 (both in P-50) oscillated more erratically than the other trees (see movie S2). Tree d13 had increased TMs with increasing distance from its rest position, but it always returned to its rest position

(yellow color pixels close to the origin in the bivariate histogram plots) between the strong gusts (Fig. 3C). Tree s13 also seemed to return to its rest position, but the crown center moved slightly to the east (Fig. 3F). Tree s15 had more constant TMs (no clear peaks) in the north-south direction (close to the wind streamwise direction); this continued over time, which suggests that the wind force was not fully transferred from the crown to the stem base after 0110 (Fig. 3, K and L). Tree s14 had a similar pattern except for a single TM peak at 1 m from the rest position in the north-south direction during the second period (Fig. 3H).

Such varying crown center positions resulted from how much an individual tree crown collided with its neighboring trees. For example, one of the P-100 trees, tree d05 collided with each of two neighbors in the streamwise direction (north-south) approximately 17,700 times (counted every 0.1 s) between 0100 and 0200 (≈50% of the time; Fig. 4A). The P-100 trees collided with each other also in the crossflow direction (east-west) approximately 40% of the time (Fig. 4B). The P-100 trees, thus, had a very high chance to collide even at lower wind speeds (0000 to 0100). On the other hand, the P-50 trees collided less than 20% of the time even between 0200 and 0300, including
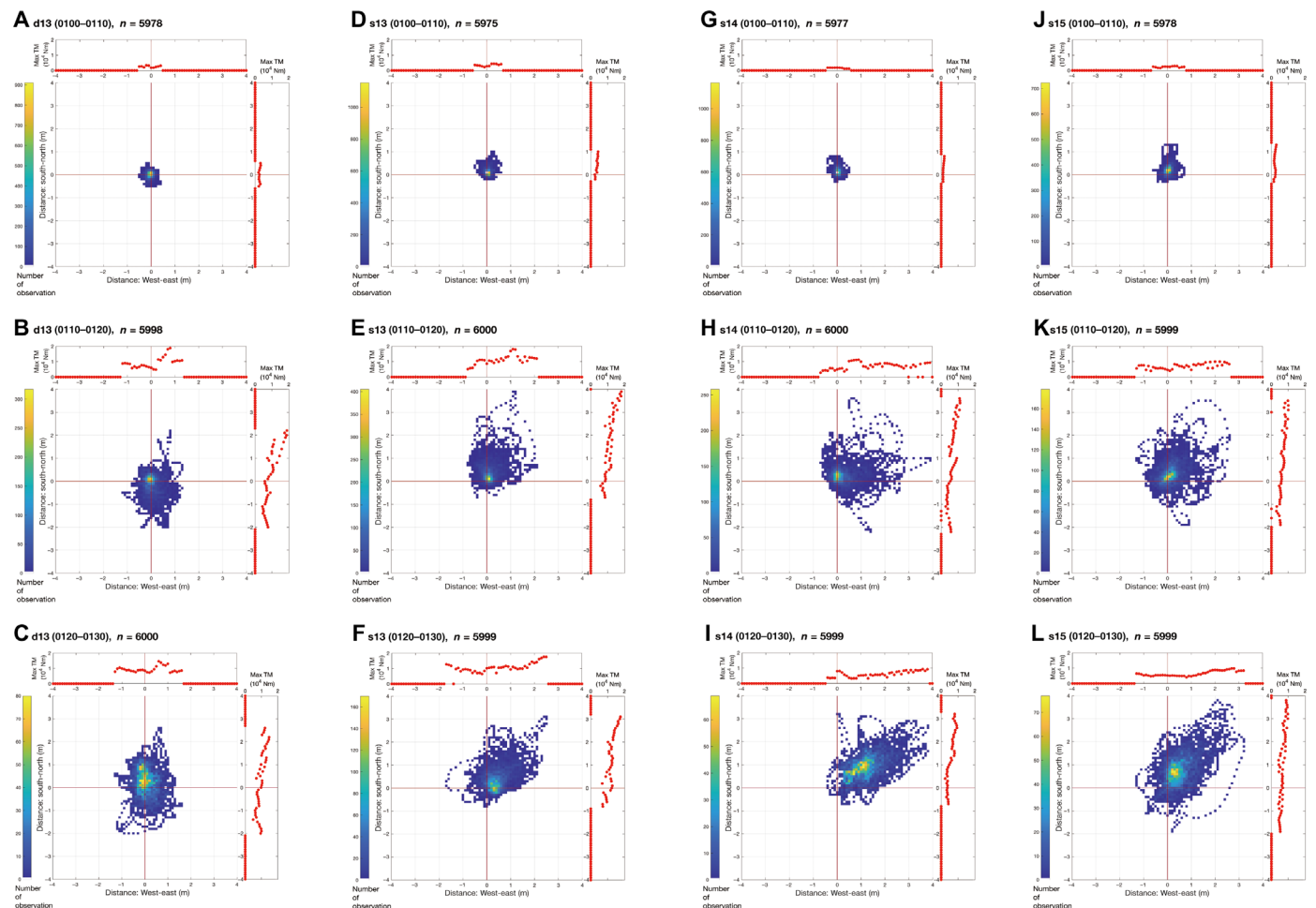

Fig. 3. Bivariate histogram plots of crown center displacement together with the maximum TMs. Displacements were calculated at a resolution of 0.1 m at the height of the crown center. The height of the crown center of d13 (**A** to **C**) is 9.62 m, s13 (**D** to **F**) is 10.15 m, s14 (**G** to **I**) is 9.50 m, and s15 (**J** to **L**) is 9.78 m. Plots of the maximum TMs at the stem base (max TM) for the north-south and east-west directions are shown as red points on the side and top from 0100 to 0130 (every 10 min). Trees d13 (in P-100) and s13 (in P-50) were undamaged, whereas trees s14 and s15 (both in P-50) were damaged.
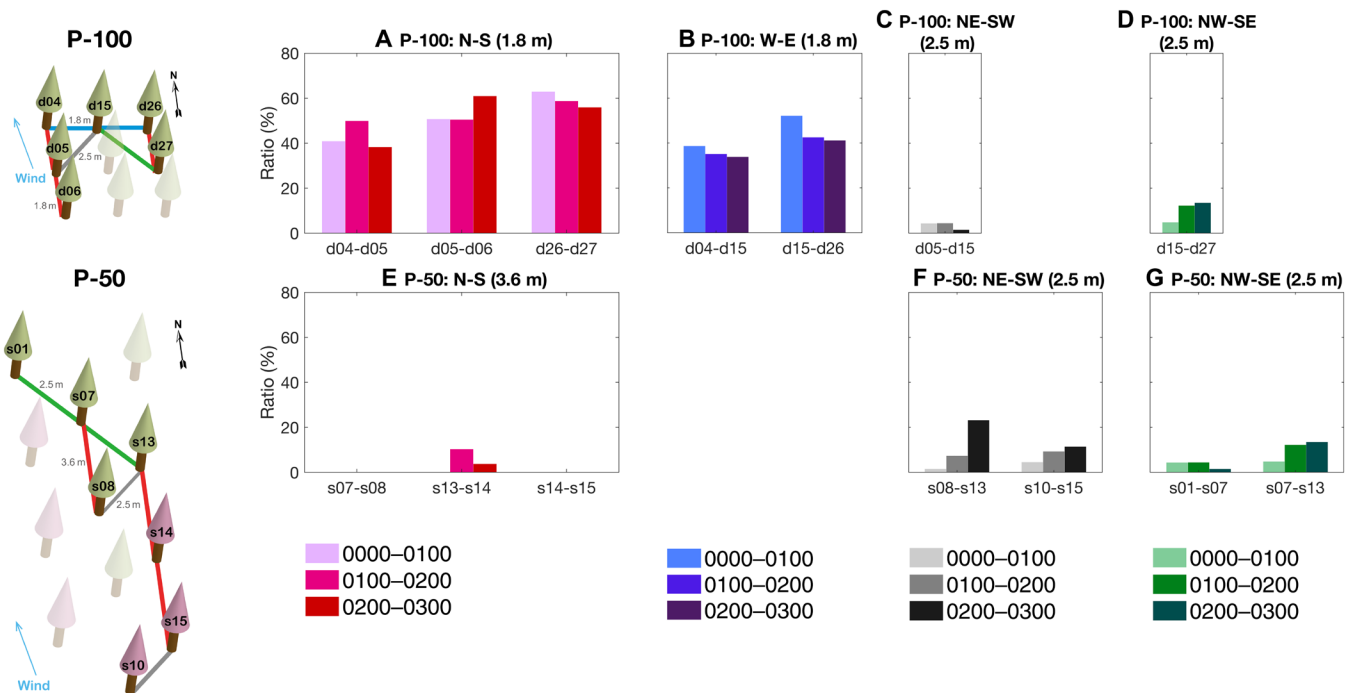
Fig. 4. Hourly ratios of crown collisions. The ratios indicate how many times the trees collided with neighboring trees over a 3-hour period (0000 to 0300 on 1 October 2018). The directions of tree collision are N-S (**A** and **E**), W-E (**B**), NE-SW (**C** and **F**), and NW-SE (**D** and **G**). The length in parentheses is the between tree distance. The collisions were determined when the distance between two tree positions at 11-m height (in the crown) was less than 0.9 m in the P-100 plot and less than 2 m in the P-50 plot. Ratios are calculated as the total number of collisions (each 0.1 s) to the total data in the hour (approximately 59 min, $n \approx 35,400$). In the tree maps (images on the left side), subject trees having 3-hour continuous data are shown with the tree ID; the red-colored trees indicate damage; and the transparent trees were excluded from this analysis due to the lack of 3-hour continuous data. NE, northeast; SW, southwest; N-S, north-south; W-E, west-east.

the peak wind speeds during the TC (Fig. 4, E to G). In the stream-wise direction, the crowns hardly ever collided simply because of the longer distance between trees (twice the P-100 inter-tree distance; Fig. 4E). The collision ratios showed the high level of support from neighboring trees in P-100 and the very low level of support in P-50. Therefore, the P-50 trees did not have a reduction in the force transfer from the crown to the stem base due to crown collisions, and this led to longer period of higher TMs (Fig. 3).

Power spectrum densities of wind components and TM
To determine the turbulent characteristics of the wind in the TC, we calculated the normalized power spectra (NPS) of the wind components (u, v, and w) and $u'w'$ every 10 min from 0100 to 0130 (Fig. 5). When the wind speed decreased in the first period (0100 to 0110; green lines), the peak frequencies became unclear especially for the u and w wind components. In the critical period (0110 to 0120; red lines), the u and v spectra peaked between 0.07 and 0.08 m^{-1} and $u'w'$ peaked at 0.1 m^{-1}. All spectra show a rapid decrease in power spectral density between 0.1 and 0.14 m^{-1}, and the turbulent decay was much steeper than the theoretical Kolmogorov decay ($-2/3$), within the inertial subrange (*22*). In the third period (0120 to 0130), the NPS lines (blue lines) for u and v moved to lower normalized frequencies (but stayed at the same absolute frequency; fig. S3), whereas those for w and $u'w'$ stayed at the same normalized frequency. The $u'w'$ spectra peaked at a similar frequency as in the previous period (0110 to 0120). When the wind speeds were lower than in this period, the peak frequencies were more likely to vary and to have a lower value, especially for u (fig. S4).

The NPS patterns of TM changed with changing wind speeds, and the P-50 trees seemed to vary more than the P-100 trees. When wind speeds initially increased (2100 to 2200), the highest NPS peaks appeared between 0.27 and 0.32 Hz (with a moving average of 0.05 Hz) in P-100 (fig. S5A). The NPS peaks in P-50 were found between 0.27 and 0.33 Hz (fig. S5B), which were less sharp than those in P-100. At frequencies above the first peak, there was a drop-in power spectral density especially in P-100, followed by a secondary peak. With increasing wind speeds (0000 to 0100), the NPS patterns became more varied for both experimental plots and the peaks were between 0.25 and 0.50 Hz in P-100 and 0.19 to 0.31 Hz in P-50. However, some of the NPS lines do not show consistently clear peaks and/or sudden decreases (fig. S5, C and D). In the critical period (0110 to 0120), on the other hand, the NPS peaks became clearer than during the previous time periods: approximately 0.42 Hz for P-100 and 0.36 Hz for P-50 (Fig. 6). Not only did the trees sway differently with the increase in wind speeds, but also the manner of sway appeared to be different between the plots. The P-50 trees tended to oscillate slowly at all times except when the wind was extremely strong, and then the peaks exceeded the previous range of peaks in the NPS during the period of lower wind speeds. However, the peaks of the P-100 trees remained at all times within the range found before the rapid increase in wind speed.

DISCUSSION
We have presented data showing how *C. japonica* trees responded to intense winds during a category-5 TC (typhoon Trami) in 2018.
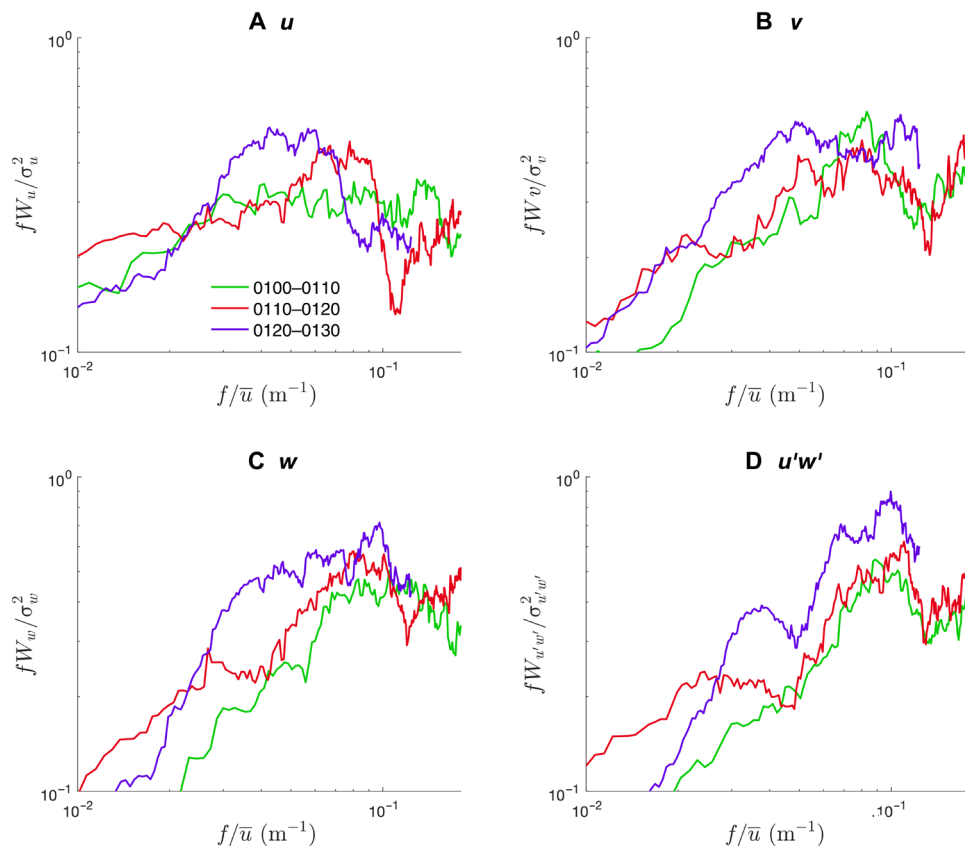
Fig. 5. NPSs of wind components. NPSs of wind components u (**A**), v (**B**), and w (**C**) and momentum flux $u'w'$ (**D**) are plotted against frequencies normalized by the mean streamwise wind speed $\bar{u}$ (m s^{-1}) every 10 min from 0100 to 0130 ($\bar{u}_{0100-0110} = 1.47$ ms^{-1}, $\bar{u}_{0110-0120} = 2.62$ ms^{-1}, and $\bar{u}_{0120-0130} = 4.04$ ms^{-1}) on 1 October 2018 (moving average over an interval of 0.01 m^{-1}).

Sustained strong winds obviously trigger damage to trees and forests, but inter-tree spacing (distance between trees) also changes the probability of failure and survival because of the different level of support provided by neighboring trees. Inter-tree spacing can be controlled through forest management, and it is also known that the risk of wind damage increases immediately after thinning treatments (*24–26*), although the exact reasons for this increase are unknown. Our findings, therefore, not only reveal tree mechanical behavior to strong winds but also provide information helpful in developing strategies for forest management to reduce the damage risk.

Different tree oscillations in different tree spacings
The trees oscillated and were displaced in a different manner between the two plots (different tree spacings) when the wind speed rapidly increased after 0110 on 1 October 2018. However, tree oscillation was very similar in the two plots when the wind speed was below 15 ms^{-1} (outside the forest, before 0110). The P-50 trees, having less support from neighboring trees than the P-100 trees, were sensitive to the rapid change of wind speed and responded quickly when the 10-min mean wind speed increased to over 25 ms^{-1} and eventually peaked at around 30 ms^{-1} in 11 hours (Figs. 1 and 2). The rapid change in wind gave rise to a sudden strong applied force, which caused the P-50 trees (wider inter-tree spacing) to oscillate with larger amplitudes, resulting in a rather irregular motion (*27–29*). On the other hand, these sudden increase in wind forces did not change the pattern of oscillations in the P-100 trees where neighboring trees

helped to dampen the oscillations. Therefore, in P-50, the trees had to individually "resist" the wind pressure so that damage depended on individual tree "stiffness." In P-100, the whole plot had an enhanced stiffness due to the support of the entire group of trees, which effectively helped to reduce the transfer of wind-induced loads down into the roots of each individual tree.

Wind force transfer from the crown to roots
A tree crown is subjected to wind loading toward the top of the tree (in the crown), creating a TM at the stem base (*30*), with the tree stem working as a lever arm attached to a root system embedded in the soil. Therefore, the TM at the stem base should increase with an increase in crown displacement if the roots are undamaged and well attached to the soil. From 0110 to 0120, the maximum TM of tree s13 (P-50) linearly increased in the streamwise direction (north-south), indicating that the roots were still attached to the soil (Fig. 3E). Tree d13 (P-100) also had an increase in the maximum TM but nonlinearly because four neighboring trees (1.8-m distance and at 90° to each other) provided good support to the tree (Fig. 4).

On the other hand, the maximum TM did not increase for trees s14 and s15 (both in P-50) with an increase in stem displacement. We assume that the wind loading (transferred from the crown to the roots through the stem) broke the roots aligned with the wind direction during the critical period (0110 to 0120). In particular, tree s14 suddenly had a reduced TM at 1 m from its rest position in the streamwise direction, suggesting the breakage of the main roots
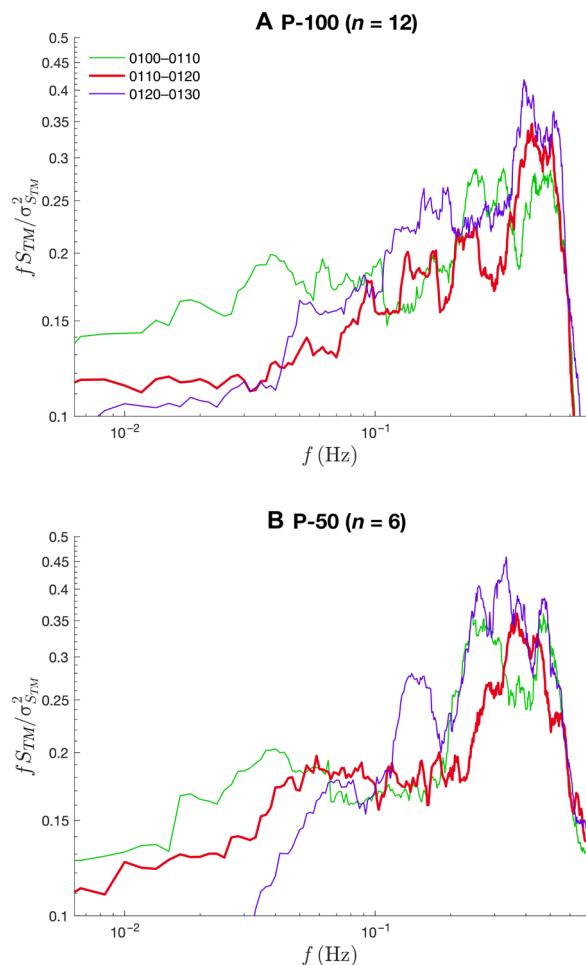
Fig. 6. Ten-minute mean NPSs of TM in the critical time period (0100 to 0130). NPSs of the 10-min mean TMs in P-100 (**A**) and P-50 (**B**) are plotted against the frequency (moving average over 0.05 Hz).

at this point (Fig. 3H). Tree s15 had a relatively constant TM over time probably due to gradual root breakage (Fig. 3, K and L). We were working with genetically similar trees planted in a small area (homogeneous soil conditions) on flat terrain; therefore, the trees had minimum variation in the proportion of large roots and root-soil plate cross-sectional area. Nevertheless, root architecture still varies (*31*) and even small difference in root architecture might change the manner of failure and alter the tree survival period in strong winds. For example, compared to the gradual root breakage of a tree such as tree s15, the main root breakage of a tree such as tree s14 allows more energy from the wind to be transmitted to the rest of the root system and leads to an increase of tree stem deformation and more rapid overturning.

Possible damage of the other P-50 trees
Before the sudden change of wind speed, the P-50 trees had already begun moving 2 hours earlier when the 10-min mean wind speed reached 10 to 13 ms^{-1} outside the forest (Figs. 1 and 2). This was much lower than the wind speed in the critical period from 0110 to 0120. Following the rapid increase in wind speed, all P-50 trees failed to return to their rest positions even after the wind had weakened (after 0500 on 1 October 2018; Fig. 1B). Probably their roots

had partly broken, resulting in their sustained displacement from their original rest positions. For example, the maximum TM of tree s13 linearly increased with an increase in distance from the rest position from 0110 to 0120 (north-south direction; Fig. 3E). However, the maximum TM became nonlinear in the next period, similar to tree d13 (Fig. 3F), although tree s13 had little support from neighboring trees unlike tree d13, which had a lot of support. Some roots of tree s13 were probably broken like trees s14 and s15, but there were not enough broken roots to allow complete overturning of the tree. Nevertheless, once trees are leaning without any support, like the P-50 trees, it is not possible to return their rest position due to the partly broken roots and the additional TM from the overhanging stem and crown. It takes time to recover vertical orientation through the growth of new roots (*32*), and this could partly explain why some trees that survive a specific TC or storm fail under much lower wind speeds in a subsequent TC or storm (*33*).

Unique to TCs or a general representation of tree damage in non-TC storms
We obtained tree damage data from a specific tree species during a particular TC. Do we also find similar dynamic behavior in different tree species and weather conditions (e.g., extratropical cyclones)? TC wind dynamics resemble non-TC winds (*34*), although TC wind fluctuations are larger than in extratropical cyclones (*35*). The NPS of the *u* component (and *w* component) decreased in magnitude very rapidly at the normalized frequencies above the peak (Fig. 5) and then increased again at higher normalized frequencies. Above the first spectral peaks, the slopes were steeper than the theoretical decay slope (−2/3), which agrees with research in a Sitka spruce [*Picea sitchensis* (Bong.) Carr.] forest (*36*), because this rapid roll-off in energy results from the spectral shortcut created by the tree canopies and tree stem that absorb energy at low frequencies and convert it to energy at higher wake and waving frequencies (*36–38*).

On the other hand, our spectral results somewhat differed from the spectra in the (undamaged) Sitka spruce forest showing steeper slopes above the peak and a narrower frequency range for the energy shortcut than in the Sitka spruce forest during an extratropical cyclone (*36*). Not only could forest and terrain conditions (e.g., tree species, tree size, tree densities, or terrain conditions) alter the spectral pattern, but also the wind speed in this TC was changing very rapidly and resulted in nonstationarity over the period of the cyclone. Nonstationary in the wind conditions might explain why the peaks in the *u* and *v* spectra unexpectedly shifted to lower normalized frequencies in the period 0120 to 0130 (Fig. 5 and fig. S3). The degree of energy transfer differs due to meteorological, tree, and forest conditions but the overall tendency of energy transfer seems a general phenomenon, especially the transfer of energy from low to high frequencies by the canopy, resulting in two visible spectral peaks with a relatively low-energy region between the two peak frequencies (*36*). The NPS also suggests that the interaction between the wind and trees is a biomechanical coupling that results in an energy exchange from the trees back into the airflow, rather than the wind spectrum within the canopy purely being controlled by the turbulent structure of the wind (*38*).

Relationship between tree resonance and damage
Does resonance between the wind and tree fundamental frequency increase the oscillation of trees and ultimately lead to tree failure in the same way as it can for man-made structures (*39*)? We did not

find resonance to cause tree damage, but rather there was strong coupling between the passage of dominant energy-carrying turbulent eddies and tree movement when the trees have little support from neighboring trees. Individual trees have their own natural frequency (*17*), and the trees in the plots swayed around the natural frequency at moderate wind speeds (fig. S5). However, once the wind speed rapidly increased with a sudden increase in the intensity of $u'w'$ (0110 to 0120), the peak frequency, especially in the P-50 trees, exceeded the range of previous frequencies, although it was slightly lower (0.36 Hz) than the peak frequency in $u'w'$ (about 0.43 Hz; see fig. S3). The peak in energy in $u'w'$ forced a new primary frequency of the P-50 tree movements, which led to efficient force transfer from the canopy to the roots and some of the P-50 trees were subsequently damaged. On the other hand, the peak frequency in the P-100 trees (0.42 Hz) stayed within the range of previous frequencies but did move closer to the peak frequency in $u'w'$. The similar peak frequencies of $u'w'$ and the P-100 trees might have produced stronger sway amplitudes through resonance, but none of the P-100 trees were damaged because of the increased forest "stiffness" created by strong interconnection between the individual tree canopies (Fig. 4). Therefore, resonance appears to be unimportant in terms of wind-caused tree damage in forests.

Main findings and future challenges

We monitored tree dynamic failure and survival during a TC and identified four key points:

1) Support from neighboring trees determined which trees failed and which trees survived, and sufficient crown interaction can increase the effective stiffness of individual trees and a whole forest stand.

2) Without support (larger between tree distances), trees oscillate individually and become more sensitive to wind speed change, transferring more wind force from the crown to the roots and resulting in soil and root fracture.

3) Resonance between the wind and tree natural frequencies appears not to be the key to tree damage in forests, but rather trees move in response to the arrival frequency of the main energy and momentum carrying gusts in the wind.

4) Tree failure in strong winds results from not only the wind turbulent structure but also the level of support that trees receive through crown collisions with neighbors, and this will be true for other tree species and forest types during any strong winds.

Understanding the dynamic nature of tree response to the wind can improve the currently available risk models (*14–16*), which incorporate tree and wind characteristics but not their full dynamic behaviors. In particular, incorporating key factors such as crown collisions, oscillation dynamics, strong wind duration, and sudden wind speed increases would improve risk model predictions. Improved models can help design damage mitigation strategies, for example, by controlling crown size and inter-tree spacing.

Our findings are also related to a long-term discussion in forestry concerning the different levels of wind damage risk for trees acclimated and unacclimated to their wind environment, and why planted trees just after thinning are more vulnerable to strong winds (*40, 41*), whereas trees following a long period after thinning are more resilient than unthinned trees (*1*). We examined trees acclimated (P-100) and unacclimated (P-50) to the wind but not trees acclimated after a long-period following thinning. The effective forest stiffness is a function of tree growth if no strong management

interventions occur. Trees suddenly losing their neighbors have only superficial crown contact with neighbors and rely on their individual stiffness to resist the wind rather than the collective stiffness of the forest. There is also increased wind penetration into the canopy. After thinning, the crown size begins to enlarge, resulting in an increasing chance of crown collision, and the stems and roots begin to acclimate to the change in wind environment. Understanding the speed of transition from a highly vulnerable forest, immediately after thinning, to a more resistant forest, following a period of adjustment and growth, is a key to developing more resilient forests in the changing climate.

MATERIALS AND METHODS
Study site

We established two research plots (figs. S1 and S6) in Chiyoda Experimental Forest of the Forestry and Forest Products Research Institute (FFPRI) in Japan (36.184°N, 140.216°E; 42 m above sea level). In 2005, 2-year-old genetically similar *C. japonica* trees (full siblings) were planted in a compartment at 1.8-m spacing (3000 trees/ha, 25 m by 22 m in size) (*42*). As a windbreak, 55 *C. japonica* trees were also planted at the compartment edge; they were genetically unrelated to the subject trees. In November 2017, we thinned some trees in half of the compartment and created two plots with a size of 15 m by 6 m: P-100 [total 24 trees, unthinned since planting, 1.8-m tree spacing, 15.7-cm mean diameter at a breast height of 1.3 m (dbh) with 2.7 cm SD] and P-50 (total 12 trees, thinned every other tree, 3.6-m mean tree spacing, 15.3-cm mean dbh with 3.3-cm SD). The means of dbh of the plots in 2017 were not significantly different at the 5% significance level (*P* = 0.7360) based on a two-sample *t* test without assuming equal variance between the plots. We also measured the tree heights of the cut trees in P-50: 13.5-m mean tree height with 1.2-m SD (*n* = 32). A buffer zone with a similar treatment surrounded each plot. When the plots were created, all trees were cut down in the other compartments located in a northeast and east direction. Subsequently, our compartment was surrounded by an open field and a 3.5-m-width paved road (on the south to southwest side; see fig. S6).

Data collection

We attached two aluminum strain transducers (*43*) at 0.25-m height on 36 trees in the north and east direction (or the west direction when we could not attach the transducer in the east direction due to the stem shape). The transducers had one active and one dummy strain gauge (KFGS-5-120-C1-23, Kyowa Inc., Tokyo, Japan) to make reliable measurements of the strain values in the tree stem without becoming detached from the growing trees. The other half of the Wheatstone bridge was completed on a circuit board with balanced precision resistors, and the whole bridge was then attached to a PhidgetBridge 1046 (Phidgets Inc., Calgary, Canada), which supplied power to the strain gauges and converted the strain to voltage. We also attached an IMU (PhidgetSpatial 3/3/3 Basic: 1042, Phidgets Inc., Calgary, Canada) to 33 tree stems in the north direction at 6-m height, which was the height from the ground surface to the initially estimated crown base. We avoided the three smallest trees due to the risk of climbing up to 6 m. The IMU includes three sensors: accelerometer, gyroscope, and magnetometer. Because the IMU uses the magnetic field, we first obtained the calibration parameters based on the local magnetic field (PhidgetSpatial User's guide;

https://phidgets.com/?&prodid=32). The signals from four strain transducers and one or two IMUs, recorded at 10 Hz, were logged by a Raspberry Pi3 (Raspberry Pi Foundation, Cambridge, UK). We used the Linux "cron" utility in the Raspberry Pi3 to control the data-logging Python codes. Data logging started running at 0 min and stopped at 59 min every hour, and the gyroscope in the IMU was reset to zero at the start of each recording period to compensate for drift.

An ultrasonic anemometer (CYG-81000, R. M. Young Co., Traverse City, USA) was attached to the top of a mast (12.5-m height: about 1.3 m lower than the mean tree height). The position was 12.6 m from the north edge and 10.8 m from the west edge of the compartment (fig. S1). It measured three orthogonal components of the wind, u, v, and w, at 1-Hz frequency, which was logged by a Graphtec data logger midi LOGGER GL240 (Graphtec Co., Yokohama, Japan). The anemometer fell off the mast at around 0210 on 1 October 2018, and we confirmed that there was useful data until 0150. We installed a three-cup anemometer (S-WSB-M003, Onset Co., Bourne, USA) at 11-m height on an electronic pylon tower (50 m north of the sonic anemometer) and recorded at 0.1 Hz. The locations are shown in fig. S6.

Wind from TC (typhoon Trami)
The Japan Meteorological Agency reported that a category-5 TC, super typhoon Trami, made landfall in Japan at approximately 2000 on 30 September 2018, and tracked north over the main island and changed to a tropical storm by 1200 on 1 October 2018 (www.data.jma.go.jp, in Japanese). The three-cup anemometer measured 29.71 ms^{-1} between 0200 and 0210 (the highest 10-min mean wind speed), and the ultrasonic anemometer recorded 4.67 ms^{-1} between 0140 and 0150 on 1 October 2018 (10-min mean wind speed inside the canopy) (fig. S7).

Field survey
After the passage of typhoon Trami, we surveyed all trees in the compartment (26 October to 21 November 2018; table S1) and found eight damaged trees including seven uprooted trees (leaning on neighboring trees) only in the area that had been thinned in the previous year. One tree, shaped like a two-tine fork, was broken at the connection between the two separate stems at 4.25-m height. We categorized trees as damaged if the minimum ratio of its angle to the ground (these calculations are explained in the following section) was less than 83% between 0600 and 0700 on 1 October 2018 (low wind speed period). For our ongoing research project, we conducted tree-pulling experiments on 37 undamaged trees in the unthinned side of the research compartment including P-100 in 2019 (see data S1). Using the averaged stem angles (recorded at 0.25- and 3-m height) at the maximum TM from the 32 uprooted trees, we determined the threshold angle for damage, which was the ratio of a mean lean angle of 14.9° (4.8° SD) away from the vertical rest position (assumed as 90°). Stem angles were based on assuming that the tree stems were always straight without any curvature due to the wind force.

We cut and logged all P-50 trees (including the buffer trees) and measured dbh, tree height, crown width and length, and stem diameter at 0.25-m height. We did not cut the P-100 trees and only measured dbh and stem diameter at 0.25-m height to continue measuring tree oscillations in the following year. We could not measure the single tree heights in P-100 from inside the plot because of the high stem density, so we measured the tree heights of three trees from outside the P-100 plot using a Vertex (Haglöf Sweden Co.,

Långsele, Sweden) in November 2018. We estimated the single tree heights in P-100 using the mean tree height of the three trees in 2018, single tree heights measured in November 2019 (data S1), and mean tree heights of the genetically related trees planted in other compartments (next to our compartment) measured in November 2017 (42). Assuming more sunlight reaching P-100 due to the absence of the thinned area and windbreak trees in the growing season in 2019, we estimated one-third growth rate from 2017 to 2018 and two-thirds from 2018 to 2019. The estimated mean tree height in 2018 showed a good agreement with the measured mean tree height of the three trees. Despite some technical problems during the TC, in total tree movement and TM data from 29 trees were successfully obtained: 20 trees in P-100 and 9 trees (including three damaged trees) in P-50 (see fig. S1); 12 trees had both the strain gauge and IMU data (some hourly datasets were missing due to the power conditions during the TC). The mean dbhs of the instrumented trees in the two plots measured after the typhoon were not significantly different at the 0.05 significance level ($P = 0.8852$).

Data processing
The strain gauge data were filtered and calibrated. First, we filtered the strain gauge output voltages using a high-pass Butterworth filter method with a 10-min cutoff frequency (44) and inserted 10-min dummy data in the first and last row of the data to avoid overfitting. The filtered data were then transformed to TMs (Nm) at the stem base using conversion parameters, which we had previously obtained in field experiments. We pulled the trees with a small non-damaging force (March and May 2018) or mechanically compressed the attached transducers (November 2018) to find the linear relationship between the strain and TM.

We rotated the IMU outputs to correct their installed x, y, and z position, which were confirmed by IMU behavior tests in the laboratory (August 2020). The three-sensor data (9-axis) were then fused using the three-sensor orientation method, which calculates quaternions of every dataset to reduce errors and noise from the local magnetic conditions. The Euler ZYX convention then computed x, y, and z coordinates at the given height. Here, we chose the center of gravity (mass) of the crown (assumed as 6 m + crown length/2) to describe the tree oscillation. Since the trees had already begun oscillating at the beginning of the study period (2000 on 30 September 2018), we used outputs from 0100 to 0200 on 28 September 2018, with no measured wind outside the plots, as the reference data to calculate the tree vertical rest positions. The stem angles to the ground were estimated by comparing the reference x, y, and z coordinates and those during the TC. The detailed calculation procedure is found in the documentation of the MATLAB Sensor Fusion and Tracking Toolbox (MathWorks Inc., Natick, USA; https://uk.mathworks.com/products/sensor-fusion-and-tracking.html).

The u, v, and w wind components, measured by the ultrasonic anemometer (2000 on 30 September 2018 to 0150 on 1 October 2018), were rotated to reduce bias from the changeable wind conditions during a strong wind. We used the double-rotation method in the coordinate rotation methods (45) to obtain the best value of the vertical component (w) (46). The process was based on 10-min averages because of the lack of stationarity in the wind conditions during the typhoon. We calculated the instantaneous momentum flux ($u'w'$) using the second rotated streamline vector u_2 and vertical vector w_2 along with $\overline{u_2}$ and $\overline{w_2}$ ($u' = u_2 - \overline{u_2}$ and $w' = w_2 - \overline{w_2}$) (22, 45).

Data analysis

We computed the crown gravity center positions in 0.1 m–by–0.1 m grids every 10 min from 2000 on 30 September 2018 to 0700 on 1 October 2018 and accumulated them in each north-south (streamwise) and east-west (crossflow) direction. The two-sample Kolmogorov-Smirnov test, which examines differences or similarity of two samples in location, dispersion, and skewness (*47*), compared the two-direction nonparametric data of paired trees within or between the plots (P-100 and P-50). We rejected the null hypothesis (two trees oscillating similarly) at the 0.05 significance level. All possible paired trees, having complete data in two directions over 11 hours, required 44,112 tests in total.

We assumed that the crowns collided when the distance between two stems at 11-m height was less than the initial open space between two crowns at the rest position. Eleven meters was determined using mean stem length to the lowest live branch after the TC (8 m), which was calculated using the measured lengths from the trees in P-50, plus half of the mean crown length, 5.86/2 m. In P-100, the threshold distance of crown collision occurrence was determined as less than 0.9 m, which was half of the stem spacing of 1.8 m, because the crowns were almost touching each other due to the close tree spacing (movie S3). We used 2.0 m for the P-50 trees, which was two times the mean crown radius of 1 m measured after the TC. We also assumed the stems to be always straight (no curvature due to the wind).

The fast Fourier transform algorithm in the MATLAB Signal Processing Toolbox (MathWorks Inc., Natick, USA) computed power spectral densities of the wind and TM at the stem base over 10-min segments to avoid errors due to nonstationary of the data (*48*). All spectra of TM were then averaged on the basis of these 10-min segments. We then normalized the power spectrum densities as frequency-weighted power spectrums divided by the signal SD (*49*).

SUPPLEMENTARY MATERIALS

Supplementary material for this article is available at https://science.org/doi/10.1126/sciadv.abm7891

View/request a protocol for this paper from *Bio-protocol*.

REFERENCES AND NOTES

1. K. Kamimura, B. A. Gardiner, S. Koga, Observations and predictions of wind damage to *Larix kaempferi* trees following thinning at an early growth stage. *Forestry* **90**, 530–540 (2017).
2. R. A. Pielke Jr., J. Gratz, C. W. Landsea, D. Collins, M. A. Saunders, R. Musulin, Normalized hurricane damage in the United States: 1900–2005. *Nat. Hazards Rev.* **9**, 29–42 (2008).
3. B. Gardiner, P. Berry, B. Moulia, Review: Wind impacts on plant growth, mechanics and damage. *Plant Sci.* **245**, 94–118 (2016).
4. S. J. Mitchell, Wind as a natural disturbance agent in forests: A synthesis. *Forestry* **86**, 147–157 (2013).
5. J. Q. Chambers, J. I. Fisher, H. Zeng, E. L. Chapman, D. B. Baker, G. C. Hurtt, Hurricane Katrina's carbon footprint. *Science* **318**, 1107 (2007).
6. D. Imbert, J. Portecop, Hurricane disturbance and forest resilience: Assessing structural vs. functional changes in a Caribbean dry forest. *For. Ecol. Manag.* **255**, 3494–3501 (2008).
7. A. Lindroth, F. Lagergren, A. Grelle, L. Klemedtsson, O. Langvall, P. Weslien, J. Tuulik, Storms can cause Europe-wide reduction in forest carbon sink. *Glob. Chang. Biol.* **15**, 346–355 (2009).
8. G. Forzieri, M. Girardello, G. Ceccherini, J. Spinoni, L. Feyen, Emergent vulnerability to climate-driven disturbances in European forests. *Nature Comm.* **12**, 1–12 (2021).
9. K. Emanuel, Increasing destructiveness of tropical cyclones over the past 30 years. *Nature* **436**, 686–688 (2005).
10. J. P. Kossin, K. A. Emanuel, G. A. Vecchi, The poleward migration of the location of tropical cyclone maximum intensity. *Nature* **509**, 349–352 (2014).
11. T.-C. Lee, T. R. Knutson, T. Nakaegawa, M. Ying, E. J. Cha, Third assessment on impacts of climate change on tropical cyclones in the Typhoon Committee Region – Part I: Observed changes, detection and attribution. *Trop. Cyclone Res. Rev.* **9**, 1–22 (2020).
12. H. C. Spatz, F. Brüchert, J. Pfisterer, Multiple resonance damping or how do trees escape dangerously large oscillations? *Am. J. Bot.* **94**, 1603–1611 (2007).
13. M. P. Coutts, Components of tree stability in Sitka spruce on peaty gley soil. *Forestry* **59**, 173–197 (1986).
14. B. Gardiner, K. Byrne, S. Hale, K. Kamimura, S. J. Mitchell, H. Peltola, J. C. Ruel, A review of mechanistic modelling of wind damage risk to forests. *Forestry* **81**, 447–463 (2008).
15. H. Peltola, S. Kellomaki, H. Vaisanen, V. P. Ikonen, A mechanistic model for assessing the risk of wind and snow damage to single trees and stands of Scots pine, Norway spruce, and birch. *Can. J. For. Res.* **29**, 647–661 (1999).
16. P. Ancelin, B. Courbaud, T. Fourcaud, Development of an individual tree-based mechanical model to predict wind damage within forest stands. *For. Ecol. Manag.* **203**, 101–121 (2004).
17. J. R. Moore, D. A. Maguire, Natural sway frequencies and damping ratios of trees: Influence of crown structure. *Trees* **19**, 363–373 (2005).
18. D. Schindler, S. Kolbe, Assessment of the response of a scots pine tree to effective wind loading. *Forests* **11**, 145 (2020).
19. E. R. Boose, D. R. Foster, M. Fluet, Hurricane impacts to tropical and temperate forest landscapes. *Ecol. Monogr.* **64**, 369–400 (1994).
20. C. J. Baker, Measurements of the natural frequencies of trees. *J. Exp. Bot.* **48**, 1125–1132 (1997).
21. D. Schindler, M. Mohr, No resonant response of Scots pine trees to wind excitation. *Agric. For. Meteorol.* **265**, 227–244 (2019).
22. B. A. Gardiner, in *Wind and Trees*, M. P. Coutts, J. Grace, Eds. (Cambridge Univ. Press, 1995), pp. 41–59.
23. M. R. Raupach, J. J. Finnigan, Y. Brunet, Coherent eddies and turbulence in vegetation canopies: The mixing-layer analogy. 78, 351–382 (1996).
24. P. S. Savill, Silviculture in windy climate. *For. Abstr.* **44**, 473–488 (1983).
25. A. D. Cameron, Importance of early selective thinning in the development of long-term stand stability and improved log quality: A review. *Forestry* **75**, 25–35 (2002).
26. C. Wallentin, U. Nilsson, Storm and snow damage in a Norway spruce thinning experiment in southern Sweden. *Forestry* **87**, 229–238 (2014).
27. N. O. Myklestad, *Fundamentals of Vibration Analysis* (Dover Publications, 2018).
28. H. Peltola, Swaying of trees in response to wind and thinning in a stand of Scots pine. *Bound. Layer Meteorol.* **77**, 285–304 (1996).
29. V. A. Webb, R. Rudnicki, S. K. Muppa, Analysis of tree sway and crown collisions for managed *Pinus resinosa* in southern Maine. *For. Ecol. Manag.* **302**, 193–199 (2013).
30. B. C. Nicoll, B. A. Gardiner, B. Rayner, A. J. Peace, Anchorage of coniferous trees in relation to species, soil type, and rooting depth. *Can. J. For. Res.* **36**, 1871–1883 (2006).
31. A. Parr, A. D. Cameron, Effects of tree selection on strength properties and distribution of structural roots of clonal Sitka Spruce. *For. Ecol. Manag.* **195**, 97–106 (2004).
32. J. Puhe, Growth and development of the root system of Norway spruce (*Picea abies*) in forest stands–A review. *For. Ecol. Manag.* **175**, 253–273 (2003).
33. K. Kamimura, S. Saito, H. Kinoshita, K. Kitagawa, T. Uchida, H. Mizunaga, Analysis of wind damage caused by multiple tropical storm events in Japanese *Cryptomeria japonica* forests. *Forestry* **86**, 411–420 (2013).
34. S. Cao, Y. Tamura, N. Kikuchi, M. Saito, I. Nakayama, Y. Matsuzaki, Wind characteristics of a strong typhoon. *J. Wind Eng. Ind. Aerodyn.* **97**, 11–21 (2009).
35. L. Li, A. Kareem, J. Hunt, Y. Xiao, C. Zhou, L. Song, Turbulence spectra for boundary-layer winds in tropical cyclones: A conceptual framework and field measurements at coastlines. *Bound. Layer Meteorol.* **154**, 243–263 (2015).
36. B. A. Gardiner, Wind and wind forces in a plantation spruce forest. *Bound. Layer Meteorol.* **67**, 161–186 (1994).
37. D. D. Baldocchi, T. P. Meyers, A spectral and lag-correlation analysis of turbulence in a deciduous forest canopy. *Bound. Layer Meteorol.* **45**, 31–58 (1988).
38. J. J. Finnigan, Turbulence in plant canopies. *Annu. Rev. Fluid Mech.* **32**, 519–571 (2000).
39. M. P. Repetto, G. Solari, Wind-induced fatigue collapse of real slender structures. *Eng. Struct.* **32**, 3888–3898 (2010).
40. K. W. Cremer, C. J. Borough, F. H. McKinnell, P. R. Carter, Effects of stocking and thinning on wind damage in plantations. *New Zeal. J. For. Sci.* **12**, 244–268 (1982).
41. A. Albrecht, M. Hanewinkel, J. Bauhus, U. Kohnle, How does silviculture affect storm damage in forests of south-western Germany? Results from empirical modeling based on long-term observations. *Eur. J. For. Res.* **131**, 229–247 (2012).
42. H. Mori, S. Ueno, T. Ujino-Ihara, T. Fujiwara, K. Yamashita, S. Kanetani, R. Endo, A. Matsumoto, K. Uchiyama, Y. Matsui, T. Yoshida, Y. Sakai, Y. Moriguchi, R. Kusano, Y. Tsumura, Mapping quantitative trait loci for growth and wood property traits in *Cryptomeria japonica* across multiple environments. *Tree Genet. Genomes* **15**, 1–15 (2019).
43. J. R. Moore, B. A. Gardiner, G. R. A. Blackburn, A. Brickman, D. A. Maguire, An inexpensive instrument to measure the dynamic response of standing trees to wind loading. *Agric. For. Meteorol.* **132**, 78–83 (2005).
44. M. Duperat, B. Gardiner, J. C. Ruel, Testing an individual tree wind damage risk model in a naturally regenerated balsam fir stand: Potential impact of thinning on the level of risk. *Forestry* **94**, 141–150 (2021).

45. A. Golzio, I. M. Bollati, S. Ferrarese, An assessment of coordinate rotation methods in sonic anemometer measurements of turbulent fluxes over complex mountainous terrain. *Atmosphere* **10**, 324 (2019).

46. J. J. Finnigan, A re-evaluation of long-term flux measurement techniques part II: Coordinate systems. *Bound. Layer Meteorol.* **113**, 1–41 (2004).

47. R. Sokal, F. J. Rohlf, *Biometry* (W. H. Freeman and Company, ed. 3, 1995).

48. R. M. Warner, *Spectral Analysis of Time-Series Data* (The Guilford Press, 1998).

49. J. C. Kaimal, J. J. Finnigan, *Atmospheric Boundary Layer Flows, Their Structure and Measurement* (Oxford Univ. Press, 1994).